RSC Advances

ROYAL SOCIETY OF CHEMISTRY

www.rsc.org/advances

Journal Name

ARTICLE

Reprobing the mechanism of negative thermal expansion in siliceous faujasite

Received 00th January 20xx,
Accepted 00th January 20xx

DOI: 10.1039/x0xx00000x

www.rsc.org/

M. P. Attfield,[a*] M. Feygenson,[b] J. C. Neuefeind,[b] T. E. Proffen,[b] T. C. A. Lucas[c] and J. A. Hriljac[c]

A combination of Rietveld refinement and pair distribution function analysis of total neutron scattering data are used to provide insight into the negative thermal expansion mechanism of siliceous faujasite. The negative thermal expansion mechanism of siliceous faujasite is attributed to the transverse vibrations of bridging oxygen atoms resulting in the coupled librations of the SiO_4 tetrahedra. The constituent SiO_4 tetrahedra are revealed to expand in size with temperature and they are also shown to undergo some distortion as temperature is increased. However, these distortions are not distinct enough in any geometric manner for the average behaviour of the SiO_4 tetrahedra not to be considered as that of a rigid units. The work displays the benefits of using total scattering experiments to unveil the finer details of dynamic thermomechanical processes within crystalline materials.

Introduction

Negative thermal expansion (NTE), or contraction, of a crystalline solid over an extended increasing temperature range is an unusual thermo-mechanical property of significant contemporary interest that has been reported for a growing number of materials, as surveyed by Lind,[1] since such behaviour was reported for the cubic oxide material ZrW_2O_8.[2] Compounds that display this property come from a variety of families of materials including condensed metal oxides and fluorides,[3] nanoporous zeolites and zeotypes,[4, 5] and metal organic framework materials.[6, 7] This thermo-mechanical property is of importance in the design of composite materials of desired thermal expansivity[1] and the performance of porous materials during their application in variable temperature adsorption, separation or catalytic processes.[8]

Determination of the NTE mechanism at the atomic level has generally been obtained from analysis of single crystal or powder X-ray or neutron Bragg diffraction data collected over wide temperature ranges. Such studies yield long range averaged crystal structures from which the interatomic distances are determined from the centres of the averaged atomic positions. As the atoms have significant thermal displacements perpendicular to the bonds, the position-averaged distances are smaller than the real values.[9] The increased thermal motion of the atoms with temperature increases the discrepancy between the averaged real distances and the position-averaged distances. This deficiency can be rectified through structural characterisation using pair distribution function (PDF) analysis of total scattering data rather than just Bragg scattering. The PDF allows determination of a materials' structure over short-, medium- and long-range length scales and yields averaged real geometric parameters instead of position-averaged geometric parameters. This technique has been widely applied to liquids and amorphous materials but is emerging as a powerful tool for studying chemical structure on the nanoscale due to the availability of new high power X-ray and neutron facilities and advances in detector technology.[10] Such studies have been able to shed new structure-specific information on the NTE mechanisms of a limited range of materials including ZrW_2O_8,[9, 11, 12] metal cyanides,[13, 14] cuprite structures M_2O (M = Cu, Ag),[15, 16] and the nanoporous siliceous zeolite chabazite.[17] The only reported PDF analysis of total scattering data performed on a zeolite, siliceous chabazite, stated that the NTE mechanism did not involve the rigid unit modes of vibration of SiO_4 tetrahedra in agreement with a previous diffraction study.[18] This non rigid behaviour of the SiO_4 tetrahedra contrasts to that often cited as being one of the primary contributors of motion involved in the NTE mechanism of several other siliceous zeolites and alumino- or gallophosphate zeotypes.[5, 19, 20] However, this study was rather limited in its scope as the material was only studied at two temperatures.[17] It was also based on X-ray scattering data rather than neutron scattering data; the latter produces better data at high Q due to the absence of angular fall-off of the scattering factors and this improves in particular the short distance part of the PDF.

[a] Centre for Nanoporous Materials, School of Chemistry, The University of Manchester, Brunswick Street, Manchester, M13 9PL, UK.
[b] Chemical and Engineering Materials Division, Oak Ridge National Laboratory, Oak Ridge, Tennessee 37831, USA.
[c] School of Chemistry, The University of Birmingham, Edgbaston, Birmingham B15 2 TT, UK.

Electronic Supplementary Information (ESI) available: Structural figure of siliceous faujasite, plots of the variation of isotropic thermal displacement parameters with temperature, plots of the variation of various geometric parameters derived from the real-space refinements as a function of temperature with estimated uncertainties included on the plots and CIF files for all refined structures. See DOI: 10.1039/x0xx00000x

Although a number of PDF studies of zeolites have been reported,[21, 22, 23, 24] there is evidently a paucity of PDF analysis studies on the NTE mechanism for zeolite materials even though this family of material is extremely important in numerous variable temperature applications. In this work we re-examine the thermo-mechanical behaviour of siliceous faujasite,[19] using structural information obtained from both Rietveld refinement and PDF analysis of total neutron scattering data to provide new insight into the NTE mechanism of this industrially relevant zeolite framework type.

Experimental

The sample of dealuminated zeolite Y (DAY) was kindly supplied by BP Amoco Chemical Company and was prepared as previously reported.[25, 26] Zero defect dealuminated Y (ZDDAY), or what we refer to as siliceous faujasite, was prepared by heating the DAY at a heating rate of 2 °C min^{-1} to 550 °C and holding the sample at 8 hr at this temperature before cooling the sample to room temperature. This process was carried out under static air and removes defects caused by dealumination. ^{29}Si MAS NMR spectroscopy determined only one type of Si site was observed at -107.2 ppm for this sample which is in good agreement with the previously reported value.[27]

0.4 g of ground siliceous faujasite was dehydrated for 8 hr at 350 °C under a vacuum of 4.8 x 10^{-7} Torr and transferred to an argon-filled glove box where it was loaded, packed down, and sealed into a 5mm diameter quartz NMR tube (Norell).

Time-of-flight total scattering neutron data were collected on the Nanoscale-Ordered Materials Diffractometer (NOMAD), the Spallation Neutron Source, Oak Ridge National Laboratory[28] which has a total flight path of 21.5 m and utilises a neutron beam collimated down to a diameter of ~6 mm. The quartz NMR tube containing the sample was held in the beam using a linear automated sample changer. Data were collected on the sample and an empty quartz NMR tube at 105, 200, 300 and 475 K using a Cobra cryostream system to cool/ heat the sample using an argon gas flow. Data acquisition times were 240 min for the sample and the empty quartz NMR tube at each temperature.

The scattering data were corrected by subtracting background scattering from the instrument and empty NMR tube, and normalizing against the corrected scattering from a solid vanadium rod. All data reduction was done using IDL routines developed for the NOMAD instrument to extract the coherent scattering data for Rietveld refinements and G(r) for the real-space Rietveld refinements using the PDF data.

Rietveld refinements were performed using data from the highest resolution detector bank 5 (*d*-range 0.2 – 1.5 $Å^{-1}$). All backgrounds were fitted using a Chebyschev polynomial fitted with twelve terms. The starting model for siliceous faujasite was taken from that reported by Hriljac *et al.*[26] The last cycle of least-square refinement included histogram scale factor, zero point, lattice parameter, three peak shape parameters, and the coordinates and isotropic thermal displacement parameters of each atom. All refinements were carried out using the EXPGUI/ GSAS suite of programs.[29, 30]

So-called 'real-space Rietveld refinements', hence referred to as real-space refinements, were performed using PDFs (G(r)) obtained by the Fourier transform of S(Q) convoluted with a Lorch function[31] with Q_{min} = 0.24 $Å^{-1}$ and Q_{max} = 31.4 $Å^{-1}$. The starting model for siliceous faujasite was taken from the structural models obtained from the Rietveld refinements at each temperature. The last cycle of least-square refinements included a scale factor, a term to account for reduction of peak width due to correlated motion, lattice parameter, and the coordinates and isotropic thermal displacement parameters of each atom. Parameters to allow for dampening and broadening of the peaks in the PDF were refined in the 105 K data set and then fixed at the obtained values for all the other higher temperature data sets. All refinements were carried out over the distance (r) range 1.34 – 40 Å using the PDFGUI suite of programs.[32] Direct fitting of certain peaks in the PDFs (G(r)) obtained by the Fourier transform of S(Q) without convolution with a Lorch function were performed using Origin software.[33]

Final observed, calculated, and difference plots for representative Rietveld and real space refinements are shown in Fig. 1. Standard crystallographic data, final atomic coordinates, isotropic atomic displacement parameters, and selected geometric parameters are given in the CIF and data files for each refinement in the ESI.

Results and discussion

The structure of siliceous faujasite is shown in ESI Fig. S1 and consists of corner-sharing SiO_4 tetrahedra. The crystal structure contains one crystallographically independent Si atom attached to four crystallographically independent O atoms. The NTE properties of siliceous faujasite derived from the two types of refinement are shown in Fig. 2. Polynomial functions are used to represent the slightly non-linear thermoresponsive behaviour of the lattice parameters. Polynomial coefficients of thermal expansion were calculated using the following expressions:

$$p = p_0 + p_1T + p_2T^2$$

$$\alpha = (p_1 + 2p_2T)/\ p$$

and the resulting coefficients are listed in Table 1. A decrease in unit cell dimension is seen over the entire temperature range 105 – 475 K with coefficents of thermal expansion (α_a) at 105 K of α_a = -6.8 x 10^{-6} K^{-1} and α_a = -5.3 x 10^{-6} K^{-1} obtained from the Rietveld and real-space refinements respectively. These values are in reasonable agreement with each other and with that reported previously (α_a = -5.4 x 10^{-6} K^{-1} at 105 K).[19]

Table 1. The experimentally determined coefficients of the polynomial functions used to fit the thermoresponsive behaviour of the unit cell parameters of siliceous faujasite.

Refinement method	Cell parameter	p_0	p_1	p_2
Rietveld	*a*	24.304	-2.043 x 10^{-4}	1.844 x 10^{-7}
Real-space	*a*	24.295	-1.516 x 10^{-4}	1.146 x 10^{-7}

The variation of various geometric parameters of the constituent SiO_4 tetrahedra and adjacent SiO_4 tetrahedra extracted from the refined crystal structures obtained from the Rietveld and real-space refinements are shown in Fig. 3 and 4, respectively.

The average Si-O bond distance obtained from the Rietveld refinements (see Fig. 3a) appears to decrease with increasing temperature. This decrease is not genuine and is an artefact of using position-averaged distances. This is confirmed from the plot of real-space derived Si-O distances (see Fig. 4a) that indicate the average Si-O bond distance actually expands with temperature as would be expected for strong Si-O bonds. The expansion in the average Si-O bond length with temperature is also seen in the directly measured average Si-O distance plotted in Fig. 5. The rates of linear expansion of the average Si-O bond distances obtained from Fig. 4a and Fig. 5 are α_l = 9.0 x 10^{-6} K^{-1} and 9.1 x 10^{-6} K^{-1} respectively that agree well with each other and lie within the range of values reported for corrected Bragg diffraction-derived Si-O bond lengths in albite (α_l = 11.7 x 10^{-6} K^{-1})[34] and those derived from PDF analysis of total scattering data, for example α_l = 5.0 x 10^{-6} K^{-1} for cristobalite[35] and α_l = 2.2 x 10^{-6} K^{-1} derived from a number of measurements of Si-O distances obtained from an assortment of siliceous materials, including two data points for a siliceous faujasite type material.[36]

The average O-Si-O bond angles of the SiO_4 tetrahedra determined from both refinements remain essentially constant (see Fig 3b and 4b) while the average O...O non-bonding distances in the SiO_4 tetrahedra obtained from the Rietveld refinements decrease with temperature (see Fig. 3c) and those from the real-space refinements increase slightly (see Fig. 4c). The variations of the average O…O distances reflect the variation of the average Si-O distances obtained from the two types of refinement.

The small variation of the averaged geometric parameters of the SiO_4 tetrahedra with temperature would allow the SiO_4 tetrahedra to be considered as rigid tetrahedra. This assumption is also supported by the fact that the individual O-Si-O bond angles determined from the Rietveld refinements are within < 6σ of each other over the whole temperature range so can be considered constant within the errors of the technique. Typically, the estimated standard deviations determined for these structures tend to be underestimated by a multiple of two to three. However, inspection of the Si-O distances, O…O non-bonding distances and the O-Si-O bond angles derived from the real space refinements indicate that the overall range of these values increase with temperature. The increasing ranges of these geometric parameters obtained from the real space refinements indicates that the peaks in the G(r) are broadening and reducing in intensity as is also seen directly in the observed G(r) at each temperature in Fig. 6. The main reasons for peak broadening and reduced peak intensity are due to increasing thermal motion or static displacements of the atoms that lead to a spread of distances and hence a broader peak in G(r). Both effects occur for siliceous faujasite. The isotropic thermal displacement parameters of all the atoms increase in a relatively smooth manner with temperature as shown in ESI Fig. S2 with the values of the O atoms being greater than the Si atom. This increase in atomic thermal motion does not fully account for the broader and less intense peaks in G(r) which is also accompanied by a non-uniform variation of the atomic positional parameters of the Si and O atoms as the temperature increases. This non-uniform variation of the atomic positional parameters results in greater distortions of the SiO_4 tetrahedra with temperature. These results suggest that the SiO_4 tetrahedra are not entirely rigid and have a greater tendency to distort as temperature increases even though they appear to be rigid in terms of the averaged parameters. A similar behaviour has been reported for the SiO_4 tetrahedra within the siliceous chabazite using PDF analysis[17] and distortions of bond angles within the constituent SiO_4 tetrahedra have been reported to occur during the α to β-phase change of the SiO_2 cristobalite system.[37]

The higher r-value structure correlation peaks in Fig. 6, for instance the peak at 3.7 Å corresponding to predominantly Si-O third neighbour distances, display a rather smooth broadening and intensity decrease with increasing temperature. This behaviour contrasts dramatically to that observed for the corresponding correlations in the siliceous chabazite[17] for which the intensity is dramatically redistributed over adjacent higher and lower r-value regions as the temperature is raised from 308 K to 753 K. This feature was reported to indicate the distortion of the SiO_4 tetrahedra in siliceous chabazite and is more severe than the changes occurring for the SiO_4 tetrahedra in siliceous faujasite supporting the notion that the SiO_4 tetraheda in siliceous faujasite are more rigid in comparison with those in siliceous chabazite as is also indicated in the Bragg diffraction studies on the two materials.[18, 19]

Geometric parameters that reflect the relative motion of the SiO_4 tetrahedra with respect to one another include the Si-O-Si bond angles and the Si…Si non-bonding distance between Si atoms in adjacent SiO_4 tetrahedra. The average Si-O-Si bond angle obtained from the Rietveld refinements (see Fig. 3d) appears to increase with increasing temperature. Again, this increase is not genuine and is an artefact of using position-averaged distances. This is confirmed from the plot of real-space derived Si-O-Si bond angles (see Fig. 5d) that indicate the average Si-O-Si bond angle actually decreases with temperature. The average Si...Si non-bonding distances between adjacent SiO_4 tetrahedra obtained from the Rietveld refinements (see Fig. 3e) decrease with temperature which is a more genuine measure of this distance due to the reduced and symmetric thermal motion of the pairs of Si atoms from which the distance is calculated. The average Si...Si non-bonding distances between adjacent SiO_4 tetrahedra obtained from the real-space refinements (see Fig. 4e) also decrease with temperature.

The results of the real-space structure refinements suggest that, over the length scale encompassing individual and pairs of SiO_4 tetrahedra, the NTE behaviour of siliceous faujasite is due to a decrease in both the average Si–O-Si angle and the accompanying average Si…Si non-bonding distance between adjacent SiO_4 tetrahedra as temperature is increased. The

averaged geometric parameters derived from the real-space refinements alone suggest that this could be a permanent deformation that contributes to NTE. Such permanent deformations have been reported to contribute to the NTE behaviour of the siliceous LTA and chabazite zeolites.[38, 39] However, consideration of the results of the Rietveld refinements in this and previous work[19] indicate the lack of any systematic changes in the O-Si-O and Si-O-Si bond angles over the temperature range (all the individual O-Si-O and Si-O-Si bond angles determined from the Rietveld refinements vary < 6σ over the temperature range). The results from both refinement types can be unified if the NTE mechanism is considered to occur via dynamic deformations of the structure. A suitable dynamic process is increasing transverse vibrations of the two-coordinate bridging O atoms in the structure; this is often considered to be one of the main contributors to one type of NTE mechanism.[1] This low energy mode of lattice vibration is readily excited at low temperatures. These vibrations lead to coupled rotations of the SiO_4 tetrahedra making up the structure of the zeolite. As the temperature is increased, the magnitude of these transverse vibrations and the resulting coupled rotations of the SiO_4 tetrahedra increase, resulting in the observed NTE as has been reported previously.[19]

Overall, the NTE mechanism of siliceous faujasite can be explained, using the averaged geometric parameters, as occurring through the coupled rigid body librations of the SiO_4 tetrahedra. However, the instantaneous behaviour of the numerous individual SiO_4 tetrahedra within the crystallites of this material are undergoing a greater degree of distortion as temperature is raised that is particularly noticeable in the PDF and missed in the standard Rietveld analysis. However, in this case these distortions are not distinct enough in any geometric manner for the average behaviour of the SiO_4 tetrahedra not to be considered that of a rigid unit.

Conclusions

The combination of Rietveld refinement and PDF analysis of total neutron scattering data have been shown to provide further insight in the NTE mechanism of siliceous faujasite. The work proves that the constituent SiO_4 tetrahedra of the material expand in size with temperature, a behaviour that was not shown directly from previous Bragg diffraction-based work. The study also reveals that some distortion of the constituent SiO_4 tetrahedra occurs as temperature is increased but on average they can be treated as rigid SiO_4 tetrahedra.

The work further displays the benefits of the total scattering technique to unveil further details of dynamic processes within crystalline materials.

Acknowledgements

The research performed at Oak Ridge National Laboratory's Spallation Neutron Source was sponsored by the Scientific User Facilities Division, Office of Basic Energy Sciences, US Department of Energy. MPA wishes to thank the Royal Society of Chemistry and the Royal Society for provision of a Journals Grant for International Authors and an International Exchange Scheme grant respectively. TCAL and JAH wish to thank Diamond Light Source for provision of a partial PhD scholarship for TCAL. We also thank G. J. Ray, Amoco Chemical Company for provision of the dealuminated zeolite-Y sample.

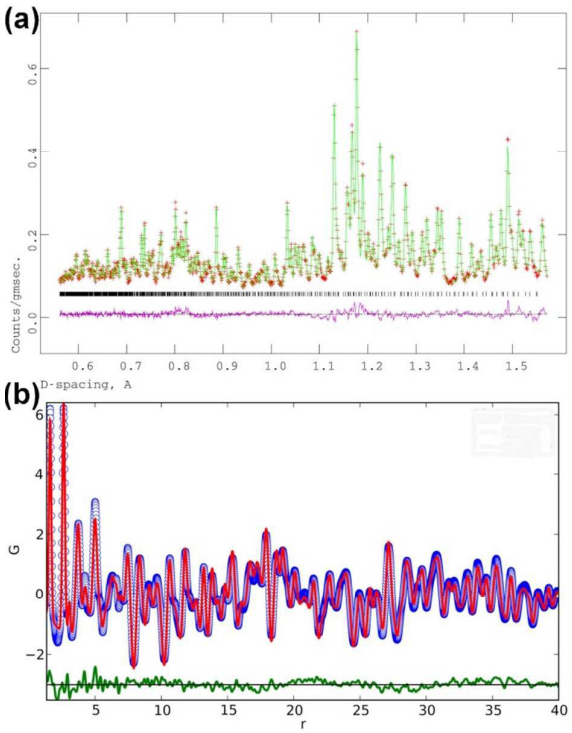

Fig.1 (a) The final observed (red crosses), calculated (green line) and difference (purple line) plot for Rietveld refinement of siliceous faujasite at 105 K. (b) The final observed (blue circles), calculated (red line) and difference (green line) plot for real-space refinement of siliceous faujasite at 105 K. The tick marks in (a) are the calcuated 2θ angles for the Bragg peaks.

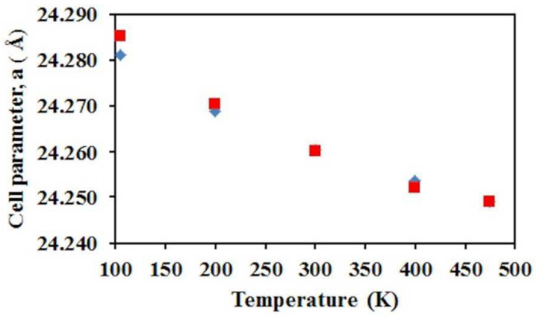

Fig. 2 The variation of unit cell parameter, *a*, as a function of temperature for siliceous faujasite. Red and blue data points correspond to unit cell parameters derived from the Rietveld and real-space refinements respectively. The estimated standard deviations fall in the ranges 0.0008 – 0.001 Å and 0.005 – 0.009 Å for the unit cell parameters derived from the Rietveld and real-space refinements respectively and are provided in the ESI.

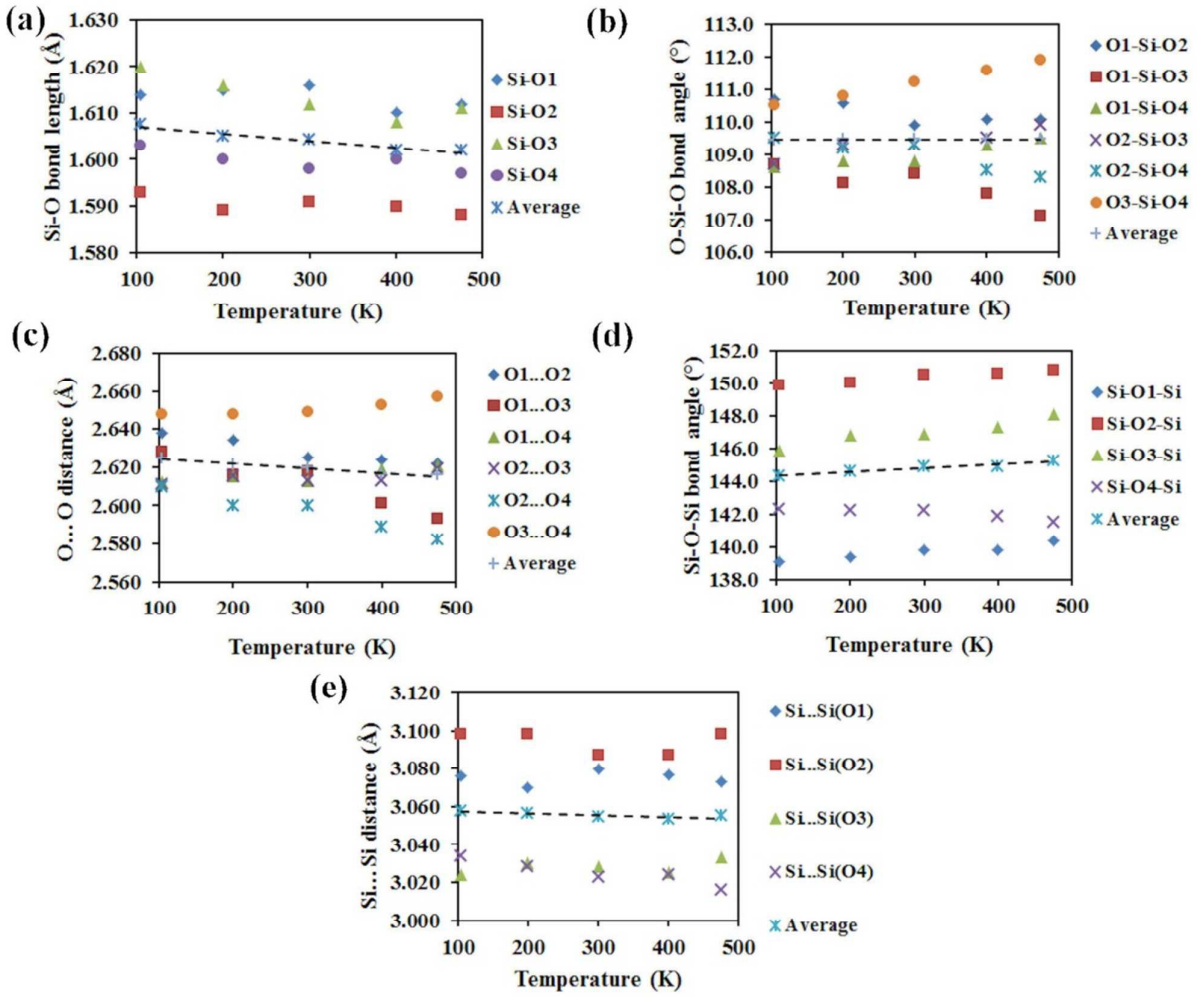

Fig. 3 The variation of various geometric parameters derived from the Rietveld refinements as a function of temperature for siliceous faujasite. Dashed lines indicate linear fits to the average parameters. The estimated standard deviations lie in the ranges 0.003 – 0.004 Å, 0.2 – 0.4 °, 0.003 – 0.005 Å, 0.3 – 0.4 °, 0.004 – 0.008 Å for the data points in (a), (b), (c), (d) and (e) respectively and are provided in the ESI.

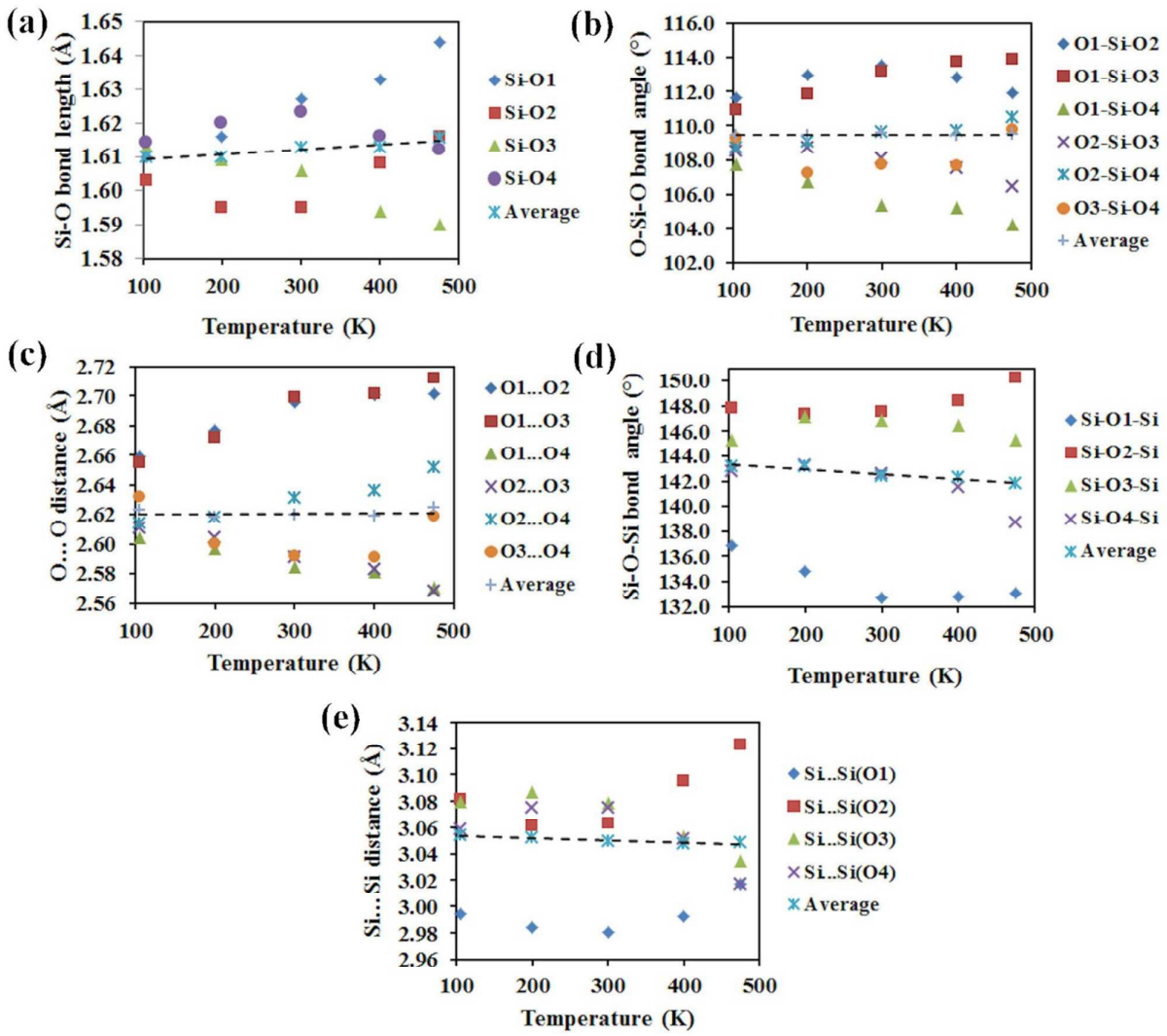

Fig. 4 The variation of various geometric parameters derived from the real-space refinements as a function of temperature for siliceous faujasite. Dashed lines indicate linear fits to the average parameters. The estimated uncertainties, calculated assuming unity uncertainties in G(r), lie in the ranges 0.04 – 0.09 Å, 3.0 – 4.8 °, 0.04 – 0.09 Å, 1.4 – 2.4 °, 0.06 – 0.09 Å for the data points in (a), (b), (c), (d) and (e) respectively and are shown in ESI Fig. S3.

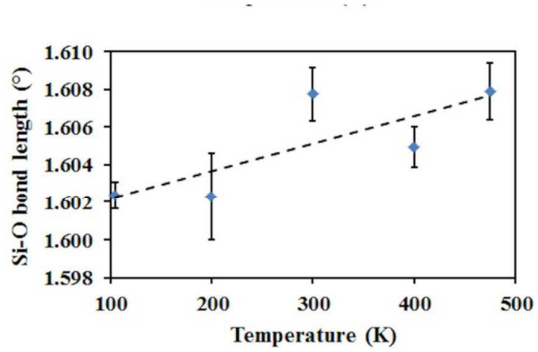

Fig. 5 The variation of the Si-O bond length derived from direct fitting of the corresponding peaks in the PDFs (G(r)) as a function of temperature for siliceous faujasite. Dashed line indicates a linear fit to the average parameters. The uncertainties lie in the range 0.001 – 0.002 Å.

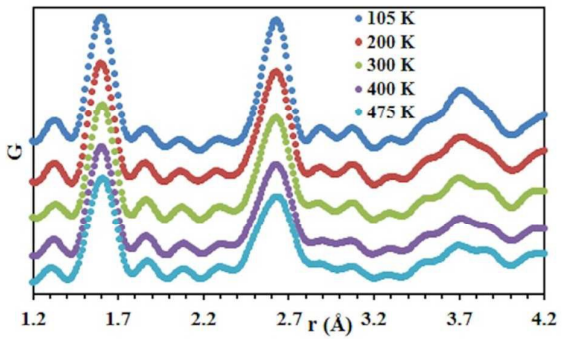

Fig.6 The observed G(r) data as a function of temperature of siliceous faujasite.

References

1 C. Lind, *Materials*, 2012, **5**, 1125.
2 T. A. Mary, J. S. O. Evans, T. Vogt, and A.W. Sleight, *Science*, 1996, **272**, 90.
3 B. K. Greve, K. L. Martin, P. L. Lee, P. J. Chupas, K.W. Chapman, and A. P. Wilkinson, *J. Am. Chem. Soc.*, 2010, **132**, 15496.
4 P. Lightfoot, D. A.Woodcock, M. J. Maple, L. A. Villaescusa and P. A. Wright, *J. Mater. Chem.*, 2001, **11**, 212.
5 M. P. Attfield and A. W. Sleight, *Chem. Mater.* 1998, **10**, 2013.
6 N. Lock, Y. Wu, M. Christensen, L. J. Cameron, V. K. Peterson, A. J. Bridgeman, C. J. Kepert and B. B. Iversen, *J. Phys. Chem. C*, 2010, **114**, 16181.
7 Y. Wu, A. Kobayashi, G. J. Halder, V. K. Peterson, K. W. Chapman, N. Lock, P. D. Southon and C. J. Kepert, *Angew. Chem. Int. Ed.*, 2008, **47**, 8929.
8 I. Bull, P. Lightfoot, L. A. Villaescusa, L. M. Bull, R. K. B. Gover, J. S. O. Evans and R. E. Morris, *J. Am. Chem. Soc.*, 2003, **125**, 4342.
9 M. G. Tucker, A. L. Goodwin, M. T. Dove, D. A. Keen, S. A.Wells and J. S. O. Evans, *Phys. Rev. Lett.*, 2005, **95,** 255501.
10 S. J.L. Billinge, *J. Solid State Chem.*, 2008, **181**, 1695.
11 M. G. Tucker, D. A. Keen, J. S. O. Evans and M. T. Dove, *J. Phys. Condens. Matter*, 2007, **19**, 335215.
12 F. Bridges, T. Keiber, P. Juhas, S. J. L. Billinge, L. Sutton, J. Wilde and G. R. Kowach, *Phys. Rev. Lett.*, 2014, **112**, 045505.
13 K. W. Chapman, P. J. Chupas and C. J. Kepert, *J. Am. Chem. Soc.*, 2005, **127**, 15630.
14 S. J. Hibble, A. M. Chippindale, A. H. Pohl and A. C. Hannon, *Angew. Chem. Int. Ed.*, 2007, **46**, 7116.
15 K. W. Chapman and P. J. Chupas, *Chem. Mater.*, 2009, **21**, 425.
16 M. Dapiaggi, H.-J. Kim, E. S. Bozin, S. J. L. Billinge and G. Artioli, *J. Phys. Chem. Solids*, 2008, **69**, 2182.
17 M.M. Martınez-Inesta and R.F. Lobo, *J. Phys. Chem. B*, 2005, **109**, 9389.
18 D. A. Woodcock, P. Lightfoot, L. A. Villaescusa, M. J. Diaz-Cabanas, M. A. Camblor and D. Engberg, *Chem. Mater.*, 1999, **11**, 2508.
19 M. P. Attfield and A. W. Sleight, *Chem. Commun.* 1998, 601.
20 M. Amri and R. I. Walton, *Chem. Mater.*, 2009, **21**, 3380.
21 H. W. Wang, D. L. Bish and H. Ma, *Am. Mineral.*, 2010, **95**, 686.
22 V. V. Narkhede and H. Gies, *Chem. Mater.*, 2009, **21**, 4339.
23 A. M. M. Abeykoon, W. Donner, A. J. Jacobson, M. Brunelli and S. C. Moss, *J. Am. Chem. Soc.*, 2009, **131**, 13230.
24 M. M. Martınez-Inesta, I. Peral, T. Proffen and R.F. Lobo, *Micropor. Mesopor. Mater.*, 2005, **77**, 55.
25 G. J. Ray, A. G. Nerheim and J. A. Donohue, *Zeolites*, 1988, **8**, 458.
26 J. A. Hriljac, M. M. Eddy, A. K. Cheetham, J. A. Donohue and G. J. Ray, *J. Solid State Chem.*, 1993, **106**, 66.
27 G. J. Ray, A. G. Nerheim, J. A. Donohue, J. A. Hriljac and A. K. Cheetham, *Colloids Surfaces*, 1992, **63**, 77.
28 J. Neuefeind, M. Feygenson, J. Carruth, R. Hoffmann and K. Chipley, *Nucl. Instr. Meth. Phys. B*, 2012, **287**, 68.
29 R. B. von Dreele and A. C. Larson, *GSAS, General Structure Analysis System*; Regents of the University of California: LANSCE, Los Alamos National Laboratory, 1995.
30 B. H. Toby, *J. Appl. Cryst.*, 2001, **34**, 210.
31 A. Soper and E. R. Barney, *J. Appl. Cryst.*, 2012, **45**, 1314.
32 C. L.Farrow, P. Juhas, J. W. Liu, D. Bryndin, E. S. Bozin, J. Bloch, T. Proffen and S. J. L. Billinge, *J. Phys.: Condens. Matter*, 2007, **19**, 335219.
33 *Origin*; OriginLab, Northampton, MA, USA.
34 R. T. Downs, G. V. Gibbs, K. L. Bartelmehs, M. B. Boisen, *Am. Mineral.*, 1992, **77**, 751.
35 M. T. Dove, D. A. Keen, A. C. Hannon and I. P. Swainson, *Phys Chem Minerals*, 1997, **24**, 311.
36 M. G. Tucker, M. T. Dove and D. A. Keen, *J. Phys.: Condens. Matter*, 2000, **12**, L425.
37 M. G. Tucker, M. P. Squires, M. T. Dove and D. A. Keen, *J. Phys.: Condens. Matter*, 2001, **13**, 403.
38 D. A.Woodcock, P. Lightfoot, L. A. Villaescusa, M. J. Diaz-Cabanas, M. A. Camblor and D. Engberg, *Chem. Mater.*, 1999, **11**, 2508.
39 T. Carey, A. Corma, F. Rey, C. C. Tang, J. A. Hriljac and P. A. Anderson, *Chem. Commun.* 2012, 5829.

TOC

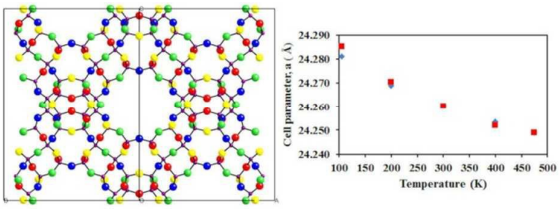

Combined Rietveld refinement and pair distribution function analysis of total neutron scattering data unveils the finer details of the negative thermal expansion mechanism of siliceous faujasite.